Optics Letters

Analysis of sinusoidally modulated chirped laser pulses by temporally encoded spectral shifting

N. H. Matlis,[1,2,4,*] A. Maksimchuk,[3] V. Yanovsky,[3] W. P. Leemans,[2] and M. C. Downer[1]

[1]University of Texas at Austin, Austin, Texas 78712, USA
[2]Lawrence Berkeley National Laboratory, Berkeley, California 94720, USA
[3]University of Michigan, Ann Arbor, Michigan 48109, USA
[4]Currently at DESY, Hamburg 22607, Germany
*Corresponding author: nmatlis@gmail.com

We present an analytical formalism elucidating how information is stored in chirped optical probes by describing the effects of sinusoidal temporal modulations on the electric field. We show that the modulations produce spectral sidebands which can be interpreted as temporal sidebands due to the time-wavelength mapping, an effect we call temporally encoded spectral shifting (TESS). A derivation is presented for the case of chirped-pulse spectral interferometry showing how to recover both the amplitude and the periodicity of the modulation from a Fourier transform of the interferogram. The TESS effect, which provides an intuitive picture for interpreting pump-probe experiments with chirped pulses, is illustrated for probing wakefields from a laser-plasma accelerator. © 2016 Optical Society of America

Detection methods based on chirped pulses have become standard for the single-shot measurement of ultrafast, time-varying phenomena because of the convenient access to the time domain offered by the time-wavelength correlation. Applications include photographing plasma waves in laser-plasma accelerators [1], diagnosing relativistic electron beams [2–5] via the mapping of terahertz-pulse waveforms [5,6], and measuring equation-of-state evolution in strongly compressed materials [7]. A complication of this approach is that the imprinting process alters the relationship between frequency and time in the probe, limiting the applicability of the wavelength as a metric of the time coordinate. It has been shown that the direct interpretation of spectral features as temporal features (i.e., "spectral encoding") results in distortions that depend on the degree of chirp and the temporal sharpness of the features [3,8,9]. This problem has been addressed in various ways, including (1) the use of spectral encoding in a regime where distortions can be neglected (which limits temporal resolution) [9], (2) use of more sophisticated analysis methods that account for the imprinting effects [3], (3) the use of

nonlinear cross-correlation with a short pulse to convert temporal features into spatial features [6], and (4) the use of frequency domain interferometry, which allows full reconstruction of the temporal field of the probe [1]. However, while the signal-recovery process has been detailed for specific scenarios, there has been no treatment of how the signal-imprinting process affects the time-frequency structure of chirped pulses in general. Thus, a heuristic picture ensures the proper interpretation and analysis of single-shot data based on chirped pulses.

Here we present a detailed analysis of how sinusoidal temporal modulations modify the structure of chirped pulses which provides a model for understanding time-varying signal-imprinting with chirped pulses in general. The signal can be imprinted onto the phase, amplitude or intensity of the probe pulse. We show that, in all cases, the modulations generate spectrally shifted copies (i.e., *satellites*) of the incident spectral field which manifest themselves in the time domain due to the probe chirp. The analysis is presented in the framework of approach 4, for which we derive analytic expressions for the modulated spectral field, the spectral interferogram, and the Fourier transform (FT) of the interferogram. We show how to extract the amplitude and frequency of a sinusoidal modulation directly from the FT and apply the results to the plasma wave measurements of [1], revealing how TESS complements the previous analysis.

It is well known that sinusoidal modulations of a carrier wave create spectrally shifted copies of the waveform, resulting in sidebands that can be used to extract the modulation signal. This effect is the basis for audio encoding in AM and FM radio and can be used for encoding signals of any frequency onto suitable carriers, e.g., terahertz information onto an optical carrier [10]. Normally, this method requires the sideband to be spectrally distinct from the carrier, which prevents modulation frequencies smaller than the probe bandwidth from being resolved. For chirped probe pulses, however, time provides an extra dimension that allows the satellites to remain isolated from the incident pulse, even when the spectral shift is significantly less than the pulse bandwidth (Fig. 1), thereby increasing the accessible modulation frequency range. These sub-bandwidth spectral shifts can be resolved as time domain sidebands by using TESS.

We start the analysis for the case of phase modulations. The generation of spectral sidebands can be easily derived for the probes

of an arbitrary electric field structure. Let $E_0(t)$ denote the temporal electric field of an unmodulated probe pulse. The modulated probe is then given by $E_{pr}(t) = E_0(t)e^{i\phi(t)}$, where $\phi(t) = \phi_0 \sin \Omega t$, and the probe spectral field is the FT of $E_{pr}(t)$:

$$\mathcal{E}_{pr}(\omega) = \frac{1}{\sqrt{2\pi}} \int_{-\infty}^{\infty} E_0(t)e^{i\phi(t)}e^{-i\omega t}dt. \qquad (1)$$

The sinusoidal phase can be expanded as a sum of carrier waves:

$$e^{i\phi_0 \sin \Omega t} = \sum_{k=-\infty}^{\infty} J_k(\phi_0)e^{ik\Omega t}, \qquad (2)$$

where the amplitudes, $J_k(\phi_0)$, are Bessel functions of the first kind. Inserting this expression into Eq. (1), we obtain

$$\mathcal{E}_{pr}(\omega) = \sum_k J_k(\phi_0)\mathcal{E}_0(\omega - k\Omega), \qquad (3)$$

where $\mathcal{E}_0(\omega)$ is the FT of $E_0(t)$ and, henceforth, sums from $-\infty$ to ∞ are implied. Equation (3) shows that the sinusoidal modulation generates a series of copies (orders) of the original spectral field, frequency-shifted by integer multiples of Ω with amplitudes that depend on the strength of the modulation, ϕ_0. Thus, the modulation is the temporal analogue of a diffraction grating.

Retrieving the temporal structure requires specification of the pulse. For simplicity, we chose a linearly chirped Gaussian pulse which can be written in the frequency domain as

$$\mathcal{E}_0(\omega) = Ae^{-\frac{1}{2}(1+i\sigma)(\frac{\omega-\omega_0}{\delta\omega})^2}, \qquad (4)$$

where $\delta\omega$ denotes the bandwidth and σ represents the chirp. Figure 1 shows that, in this case, the original pulse and the generated satellites appear as diagonal strips in time-frequency (t, ω) space. Due to the chirp, the instantaneous bandwidth of each strip (i.e., the spectral width of each order in the $t = 0$ lineout) is significantly less than the original temporally integrated bandwidth, (i.e., the spectral width, $\delta\omega$, of the spectral projection of any order), allowing the bands to remain isolated even when $\Omega < \delta\omega$. Notice also that time-lineouts intersect multiple orders, but at distinct temporal locations, which is the
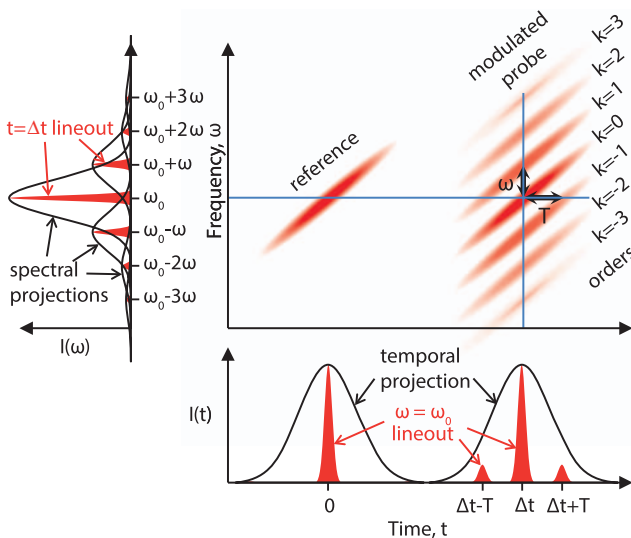
Fig. 1. Depiction of the time-frequency representation of a linearly chirped probe pulse modulated by a sinusoidal temporal phase of frequency Ω and an identically chirped, but unmodulated and temporally shifted, reference pulse.

basis for TESS. Techniques that integrate the probe in time or frequency clearly will not resolve the details of the diagonal structure. However, by doing spectral interferometry with a similarly chirped, but delayed, reference pulse, the important coordinate becomes the *relative delay*, which is independent of wavelength for linearly chirped pulses. An FT of the spectral interferogram effectively provides a histogram of energy versus relative delay, allowing integration over frequency without destroying the time structure.

The reference pulse is given by $E_r = E_0(t - \Delta t)$, which, in the spectral domain becomes $\mathcal{E}_r(\omega) = \mathcal{E}_0(\omega) \exp i\omega\Delta t$. The spectral interferogram has the form: $\mathcal{S}(\omega) = |\mathcal{E}_{pr}(\omega)|^2 + |\mathcal{E}_r(\omega)|^2 + \mathcal{E}_{pr}(\omega)\mathcal{E}_r^*(\omega) + $ c.c., which expands to

$$\mathcal{S}(\omega) = \sum_{n,m} J_n(\phi_0)J_m(\phi_0)\mathcal{E}_0^*(\omega - n\Omega)\mathcal{E}_0(\omega - m\Omega) + |\mathcal{E}_0(\omega)|^2$$

$$+ \sum_k J_k(\phi_0)\mathcal{E}_0^*(\omega)\mathcal{E}_0(\omega - k\Omega)e^{-i\omega\Delta t} + \text{c.c.} \qquad (5)$$

The interferogram contains contributions from all possible pairings of the probe orders and the reference. The first term represents the set of interferences of the orders with each other, the second term is the reference self-interference, and the third and fourth terms represent the interferences between the probe orders and the reference. In the spectral domain, all of these terms overlap, making it impossible to isolate a particular pairing but, by transforming to the time domain via an FT, the terms get organized according to the temporal delay between the two interfering elements. The FT of the interferogram is

$$S(t) = \sum_m g_m(\phi_0, t, \Omega)H(t, m\Omega) + H(t, 0)$$

$$+ \sum_k J_k(\phi_0)H(t - \Delta t, k\Omega) + \text{c.c.}, \qquad (6)$$

$$H(t, \Omega) \equiv \frac{1}{\sqrt{2\pi}} \int_{-\infty}^{\infty} \mathcal{E}_0^*(\omega)\mathcal{E}_0(\omega - \Omega)e^{i\omega t}d\omega \qquad (7)$$

$$g_m(\phi_0, t, \Omega) \equiv \sum_n J_n(\phi_0)J_{m+n}(\phi_0)e^{in\Omega t}. \qquad (8)$$

From the fundamental theorem of FTs, the function $H(t, \Omega)$ represents the time domain convolution between the reference and an order shifted by Ω. When $\phi_0 = 0$, the FT has a well-known three-peak structure [Fig. 2(a)] given by $S(t) = 2H_0(t) + H_0(t - \Delta t) + H_0(t + \Delta t)$, where

$$H_0(t) \equiv H(t, 0) = \delta\omega \frac{A^2}{\sqrt{2}} e^{i\omega_0 t}e^{-\frac{1}{4}(t/\delta t)^2}, \qquad (9)$$

and $\delta t \equiv 1/\delta\omega$ is the coherence time of the pulse. The side peaks at $t = \pm\Delta t$ correspond to the reference-probe interference terms which, in general, are used to extract the phase information from the experiment. Equation (6) shows that, when $\phi_0 \neq 0$, the structure of the side peak is modified, yielding a series of satellites [Fig. 2(b)] described by

$$H(t, k\Omega) = f(k\Omega)e^{\frac{1}{2}ik\Omega t}H_0(t + \mu k\Omega), \qquad (10)$$

which are temporally shifted copies of the unmodulated side peak scaled by $f(k\Omega) = \exp\{-\frac{1}{4}(\frac{k\Omega}{\delta\omega})^2\}$. The factor, $\mu \equiv \sigma/\delta\omega^2$, is a proportionality constant that relates frequency to time in the chirped pulse. The temporal representation of the spectral shift, Ω, is thus given by $T \equiv \mu\Omega$. The function $f(k\Omega)$ describes the degree of the spectral overlap between the kth order and the

reference and, therefore, defines via the factor μ the time window in the FT where interference information can be stored. Thus, when $\Omega \gg \delta\omega$, TESS is ineffective since $f(\Omega) \approx 0$. In this case, however, TESS is not needed since the spectral shift is larger than the bandwidth and can be detected directly from the spectrum. To extract TESS information, the satellites must be distinguishable from each other (i.e., $T > \delta t$), which allows the modulus squared of the FT to be written, ignoring cross terms as

$$|S(t)|^2 = \sum_m |g_m^2(\phi_0, t, \Omega)|^2 f^2(m\Omega)|H_0(t+mT)|^2 + |H_0(t)|^2$$
$$+ \sum_k J_k^2(\phi_0) f^2(k\Omega)|H_0(t-\Delta t+kT)|^2 + |c.c.|^2, \quad \textbf{(11)}$$

where $|c.c.|^2$ describes structure in the negative time domain. Satellites of the central peak (at $t = mT$) are also created by the probe orders interfering with each other, as described by the first term of Eq. (6). In this case each satellite is the sum of all order-order pairings with the same difference m in the order parameter. The interference modulates the envelopes, described by $|g_m(\phi_0, t, \Omega)|^2$ which has zeros at $t_j = 2\pi j/\Omega$, where j are integers.

Although, in principle, Eq. (11) shows that infinitely many satellites are generated by the modulation, in practice, often only the $m = 0, 1$ and $k = 0, \pm1$ peaks will be detectable. To extract the frequency of the modulation, the chirp factor μ must be well characterized. Then Ω can be determined from the time difference, T, between the $k = \pm1$ and $k = 0$ peaks. The modulation strength, ϕ_0, can be extracted from the ratio, β, of the $k = \pm1$ and $k = 0$ peak amplitudes in $|S(t)|^2$ by inverting $\beta = f^2(\Omega)(J_1(\phi_0)/J_0(\phi_0))^2$ to get $\phi_0 \approx \sqrt{4\{\beta/f^2(\Omega) + 1/4\}^{1/2} - 2}$. The absolute peak amplitudes should not be used to extract ϕ_0 because, unlike β, they are affected by factors such as intensity and alignment mismatches between the probe and reference.

For small modulations, this formalism can be extended to phase shifts of an arbitrary form using $e^{i\phi(t)} \approx 1 + i\phi(t)$, resulting in: $\mathcal{E}_{pr}(\omega) \approx \mathcal{E}_0(\omega) + \frac{i}{\sqrt{2\pi}}\int_{-\infty}^{\infty}\Phi(\xi)\mathcal{E}_0(\omega - \xi)d\xi$, where $\Phi(\xi)$ is the FT of $\phi(t)$. A comparison with Eq. (3) shows

a)

b)

Fig. 2. Modulus squared of $S(t)$ on a log scale. Only the $+t$ side is shown, since $S(t)$ is symmetric about $t = 0$. (a) Unmodulated probe. (b) Modulated probe for $\phi_0 = 1$, $\sigma = 10$, and $\Omega/\delta\omega = 1$. The dotted blue and solid red lines are the spectral overlap functions for the 1st and 2nd orders, respectively.

that the modulation creates a continuum of copies of the original spectral field shifted by ξ. The side peak term [i.e., 3rd term of Eq. (6)] becomes $S(t)_{side} \approx H_0(t - \Delta t) + \frac{1}{\sqrt{2\pi}}\int_{-\infty}^{\infty}\Phi(\xi)f(\xi)H_0(t - \Delta t + \mu\xi)d\xi$, showing that the frequency content, $\Phi(\xi)$, of the modulation gets mapped onto time by the TESS effect. More precisely, the satellite generated by the modulation (2nd term of $S(t)_{side}$) is the convolution of $H_0(t)$ with the time domain mapping of $\Phi(\xi) \times f(\xi)$, which represents the modulation spectrum in the time domain.

The formalism for amplitude and intensity modulations is similar to that of phase modulations. The amplitude modulations can be written as $E_{pr}(t) = E_0(t) \times (1 + a_0 \cos \Omega t)$, so that Eq. (3) becomes $\mathcal{E}_{pr}(\omega) = \Sigma_k A_k(a_0)\mathcal{E}_0(\omega - k\Omega)$, where $A_0 = 1$, $A_{\pm1} = a_0/2$ and $A_{|k|\geq2} = 0$. The rest of the analysis is then identical to the phase case, except that $J_k(\phi_0)$ must be replaced with $A_k(a_0)$. Similarly, the intensity modulations can be expressed by $I_{pr}(t) = I_0(t) \times (1 + b_0 \cos \Omega t)$, where $I_{pr}(t) = |E_{pr}(t)|^2$ and $I_0(t) = |E_0(t)|^2$ are the probe modulated and unmodulated temporal intensity profiles, respectively. The modulated spectral field can be expressed using only two terms as $\mathcal{E}_{pr}(\omega) = \Sigma_k B_k(b_0)\mathcal{E}_0(\omega - k\Omega)$, where $B_0^2 + B_{-1}^2 = 1$, $2B_0 B_{-1} = b_0$, and all other coefficients are zero. As in the amplitude case, $J_k(\phi_0)$ must be replaced with $B_k(b_0)$.

To demonstrate the concepts presented here, TESS was used to reanalyze the data obtained from previous experiments in the imaging of plasma waves from a laser-plasma accelerator (LPA) [1]. LPAs are compact accelerators which use intense ($\sim10^{18}$ W/cm²) short (~30 fs) laser pulses to excite plasma-density waves (wakefields) which can accelerate electrons with gradients (~100 GeV/m) that far exceed those of conventional accelerators. The amplitude and frequency of the plasma waves, which are sensitively affected by the highly nonlinear interaction of the laser pulse with the plasma, govern the behavior of the accelerator and, thus, are important to characterize. The wakefields were generated by focusing the intense pump pulses onto a supersonic jet of helium gas. The leading edge of the pump photo-ionized the gas, generating a sharp transition in electron density known as an ionization front, followed by periodic wakefield oscillations in the electron density. A synchronized, linearly chirped probe pulse at 400 nm copropagated with and temporally overlapped both the ionization front and the wake oscillations, resulting in temporal modulations of the probe phase. A second linearly chirped pulse preceded the probe by two picoseconds and was used as a reference for the interferometry.

In the original analysis [1], frequency domain holography (FDH) was used to reconstruct the temporal electric field of the probe pulse, resulting in detailed images of the 2D spatio-temporal structure of the wakefields. Thus, critical features such as wakefield curvature and periodicity were obtained [Fig. 3(a)]. A disadvantage of FDH, however, is that the wakefield images are formed from an average of the structures generated at each longitudinal location of the interaction. Therefore, longitudinal variations in the wakefield periodicity caused by plasma-density gradients resulted in a measured wakefield amplitude which was significantly smaller than the maximum generated, an effect confirmed by simulation [1].

TESS, which requires only a single FT operation, offers a complementary analysis that allows access to different aspects of the information stored in the data. Although no images are formed, information about both the wakefield frequency and amplitude are obtained. Figure 3(b) shows the TESS analysis for the wake image shown in Fig. 3(a). The $k = -1$ and $k = +1$ satellites are
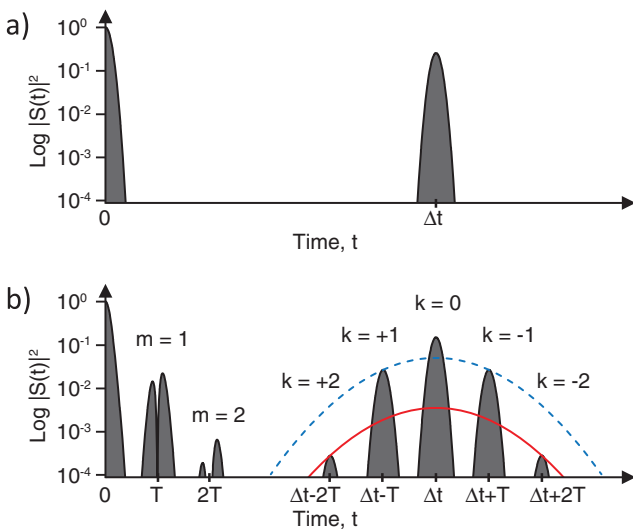
clearly visible, with a transverse spatial extent that matches the wakes in Fig. 3(a). The broad feature extending to the left of the side peak, from 2.0 down to 1.4 ps is caused by the ionization front, which strongly shifts the portion of the probe spectrum that it overlaps. Since the ionization front is step-function-like, the spectral shifting is broad and asymmetric in the blue direction, which corresponds to the left side of the $k = 0$ peak for our chirp. The large degree of spectral shifting translates to a large range of delays in the FT, due to the TESS effect, which is what is seen. In addition, as expected, the spatial extent of this broad feature co-incides with that of the plasma in 3(a). The ionization front and wakefield features are also visible in the $m = 1$ satellite to the right of the central $t = 0$ peak. In this case, the multiple elements of $g_m(\phi_0, t, \Omega)$ interfere with each other, causing time domain fringes. The vertical bands at 0.8, 1.25, and 2.9 ps are noise features from prepulses in both the probe and reference.

The wake amplitude was determined from the $k = -1$ peak, which was not obscured by the ionization-front feature. A modulation strength of $\phi_0 = 0.8$ rad was obtained for the wake in 3(a),

corresponding to a wake amplitude of $\delta n_e / n_e \approx \phi_0 c\omega / L\omega_p^2 \approx 0.1$, where $L \approx 1.5$ mm was the interaction length, and c is the speed of light. For comparison, the wake amplitude recovered from Fig. 3(a) was only $\delta n_e / n_e \approx 0.055$. Since contributions to the $k = \pm 1$ satellites from target regions with differing plasma densities do not overlap in the FT, the averaging issue experienced with FDH is to an extent mitigated; thus, a larger estimate of the wake amplitude from the TESS analysis is to be expected.

The dependence of the wake frequency on electron density, $\omega_p(n_e)$, was also determined from the position of the $k = -1$ peak [Fig. 3(c)], mirroring the analysis of Matlis *et al.* [1], using FDH-generated wake images. The TESS effect can be clearly seen in the movement (from 2.2 to 2.7 ps) of the $k = \pm 1$ satellites with density. The dashed lines indicate the expected satellite locations, assuming $\Omega = \omega_p$, where ω_p is the plasma frequency. In Fig. 3(d), the $k = -1$ satellite positions (red dots) were used to compute the $k = +1$ satellite locations (blue squares), to confirm their symmetric placement about the $k = 0$ peak and to help distinguish the $k = +1$ wake from ionization-front features.

In conclusion, our analysis allows a connection to be drawn between the frequency of a temporal modulation and the position of the corresponding signal in the time domain of the FT. This connection enables interpretation of the complex features in the FT which can improve the extraction of information, even for cases where the modulations are not sinusoidal. The interpretation is particularly important for defining limits for numerical window-ing in the processing of spectral interferograms. The analysis pre-sented here demonstrates clearly that the information about the modulations is *not* contained in the primary side peak of the FT, as is often assumed, but rather in the satellites, which may be significantly separated from the primary peak in the time domain.

Fig. 3. (a) FDH reconstruction showing a wakefield, plasma, and ionization front. (b) $|S(t,y)|^2$ for the data in (a). (c) $|S(t)|^2$ versus n_e for the $y = 0$ location in (b). The dashed lines represent the expected $k = \pm 1$ locations for $\Omega = \omega_p$. (d) Waterfall plot representation of the data in (c). The red dots and blue squares indicate the $k = -1$ and $+1$ peaks, respectively, where the $k = +1$ peak locations were inferred from the $k = -1$ peaks.

REFERENCES

1. N. H. Matlis, S. Reed, S. S. Bulanov, V. Chvykov, G. Kalintchenko, T. Matsuoka, P. Rousseau, V. Yanovsky, A. Maksimchuk, S. Kalmykov, G. Shvets, and M. C. Downer, Nat. Phys. **2**, 749 (2006).
2. I. Wilke, A. M. MacLeod, W. A. Gillespie, G. Berden, G. M. H. Knippels, and A. F. G. van der Meer, Phys. Rev. Lett. **88**, 124801 (2002).
3. B. Yellampalle, K. Y. Kim, G. Rodriguez, J. H. Glownia, and A. J. Taylor, Appl. Phys. Lett. **87**, 211109 (2005).
4. J. van Tilborg, C. B. Schroeder, C. V. Filip, C. Tóth, C. G. R. Geddes, G. Fubiani, R. Huber, R. A. Kaindl, E. Esarey, and W. P. Leemans, Phys. Rev. Lett. **96**, 014801 (2006).
5. N. H. Matlis, G. R. Plateau, J. van Tilborg, and W. P. Leemans, J. Opt. Soc. Am. B **28**, 23 (2011).
6. S. P. Jamison, J. Shen, A. M. MacLeod, W. A. Gillespie, and D. A. Jaroszynski, Opt. Lett. **28**, 1710 (2003).
7. A. Benuzzi-Mounaix, M. Koenig, J. M. Boudenne, T. A. Hall, D. Batani, F. Scianitti, A. Masini, and D. Di Santo, Phys. Rev. E **60**, R2488 (1999).
8. J. R. Fletcher, Opt. Express **10**, 1425 (2002).
9. X.-Y. Peng, O. Wili, M. Chen, and A. Pukhov, Opt. Express **16**, 12342 (2008).
10. J. van Tilborg, D. J. Bakker, N. H. Matlis, and W. P. Leemans, Opt. Express **19**, 26634 (2011).